communications physics

ARTICLE

https://doi.org/10.1038/s42005-023-01197-x OPEN

Microresonator-based electro-optic dual frequency comb

Nicholas J. Lambert [1,2]✉, Luke S. Trainor [1,2] & Harald G. L. Schwefel [1,2]✉

Microresonator based dual frequency combs offer an integrated photonic solution to a wide range of technological challenges, including spectroscopy, range finding, material characterization and hyperspectral imaging. These applications require a high level of mutual coherence between combs, but achieving such stability can be demanding. Here we experimentally demonstrate that comb generation exploiting the rich structure of the nonlinear electro-optic tensor in lithium niobate can generate ultra-stable dual combs, with the two combs naturally having orthogonal polarizations. We theoretically explore the application of our technique to dual frequency comb generation from the far infrared (IR) to the ultraviolet (UV). Our combs have relative linewidths as low as ~400 μHz, and require no stabilization or post-processing methods.

[1] Department of Physics, University of Otago, Dunedin, New Zealand. [2] The Dodd-Walls Centre for Photonic and Quantum Technologies, Dunedin, New Zealand. ✉email: nicholas.lambert@otago.ac.nz; harald.schwefel@otago.ac.nz

Optical frequency comb generators emit short coherent pulses of light with a stable repetition rate. Equivalently, the generated light spectrum comprises many discrete frequencies spaced by this same repetition rate. These precision light sources have become ubiquitous in applications of photonic technologies[1–6] because they allow coherent sampling over a broad part of the optical spectrum[7]. The addition of another comb to the frequency spectrum, with a slightly different line spacing, results in the generation of a *dual comb*. A dual frequency comb allows one comb to be used as a probe and the other to be used as a reference against which the probe can be compared. It can be applied in many scenarios in which optical interferometric techniques are commonly used; by measuring the beat frequencies between close-in-frequency comb lines, analysis can take place in the radio-frequency (r.f.) part of the electromagnetic spectrum, allowing fast and economical measurements[8,9]. They have been demonstrated as compact solutions for digital holography[10], spectroscopy[11–13], range finding and optical depth measurements[14], and optical coherence tomography[15].

To exploit some of these techniques in full, a narrow relative linewidth between the comb line pairs[8,16] is required. This precise synchronization between the combs permits long coherent averaging periods, improves sensitivity, and increases signal-to-noise ratios. For instance, the distance uncertainty for dual comb based distance measurements[17,18] is proportional to the optical phase uncertainty of the comb lines[19]. Furthermore, common techniques for broadening frequency combs to increase the number of comb lines also require an initial frequency comb with low phase noise[20]. Tight locking of two pulsed lasers provides a stable spectrum[11,21], but comes with high complexity and cost, making operation outside of a laboratory environment difficult. Analogue[22] and digital[23] correction techniques have also been applied, but increase the data handling requirements. The generation of stable dual combs therefore remains an important challenge.

Nonlinearities due to the third-order susceptibility $\chi^{(3)}$ have been used extensively to produce solitonic behaviour in the propagating light field, allowing the generation of Kerr-soliton frequency combs[24–26]. Dual Kerr combs have been demonstrated[12], including separable counter-propagating dual combs[27,28], but require sophisticated techniques for stabilization[29]. Optical second order $\chi^{(2)}$ nonlinearities have also been used for comb generation, through cascaded optical parametric oscillation and sum-frequency generation[30–37]. Here, we instead use an electro-optic $\chi^{(2)}$ nonlinearity via cascaded sum- and difference-frequency generation between the optical carrier and an incident microwave drive tone[38–40]. Because the comb line spacing is given by the microwave frequency, this technique allows more straightforward control of comb repetition rates. By applying two microwave tones simultaneously, dual[7,41] and dual-driven combs can be generated[42].

Here we present a straightforward method of generating electro-optic dual combs in a microresonator using a single continuous-wave laser source. It makes use of the optical mode structure in microresonators to generate two combs of orthogonal polarization, allowing them to be easily separated into separate beam paths. Our device exploits whispering gallery modes (WGMs) supported by a nonlinear optical microresonator[43,44]. The even spacing and high Q of these modes makes them a natural platform for efficient frequency comb generation, and the nonlinearity allows the generation of new frequencies.

Results and discussion

Figure 1b shows a schematic illustration of our implementation. At the core of our device is a ring-shaped microresonator made from mechanically polished x-cut lithium niobate ($LiNbO_3$)[45–47] (see 'Methods'). The WGMs ($Q \sim 10^8$) are first driven with swept laser light at a wavelength close to 1550 nm, resulting in the mode spectra shown in Fig. 1e. The resonator can support two optical mode families with different free spectral ranges; axial modes, in which the electric field is normal to the plane of the resonator, and radial modes, for which the electric fields lies in the plane of the disc. Unlike $LiNbO_3$ resonators with the z-axis normal to the plane of the WGMs, an x-cut resonator has a point on its rim for which the wavevector of light of both polarizations is equal. This allows efficient evanescent coupling to both axial and radial modes using light with the same angle of incidence.

To permit the generation of new optical frequencies, the optical microresonator is embedded in a toroidal loop gap microwave cavity (Fig. 1b, c, see 'Methods' and Supplementary Note 2). The electric field vector of the lowest order microwave mode is constant in magnitude around the torus, and points between the inner and outer of the cavity. It is therefore aligned with the radial axis of the microresonator. By fashioning a sharp edge on the outer surface of the loop capacitance, we focus the electric field into the optical mode volume, increasing the overlap between optical and microwave fields. The microwave cavity mode has a centre frequency of 7.87 GHz (Fig. 1d), lying between the free spectral ranges (FSRs) of the radial and axial mode families. By driving the cavity at one of these FSRs using a coupled antenna, a frequency comb can be generated; by driving it simultaneously at both FSRs, a dual comb results.

The interaction of different frequencies in nonlinear materials generally requires careful consideration of phase-matching, in order to preserve both energy and momentum[44]. This requirement is encapsulated by the expression for the coupling rate g between the complex electric fields of the input optical and microwave modes, E_{in} and E_{Ω} respectively, and that of the mode E_{out} at the generated optical frequency,

$$g \propto \int_{\substack{\text{mode}\\ \text{volume}}} \chi^{(2)} E_{\mathrm{in}} E^{*}_{\mathrm{out}} E_{\Omega} dV. \tag{1}$$

Here, the mode volume integral runs around the resonator. Because the input and output modes are orthogonal, spatially uniform microwave modes and electro-optic coefficients lead to $g = 0$. Therefore, for efficient comb generation, either the microwave mode or the electro-optic coefficient must have an antisymmetric spatial component.

In previous work using z-cut $LiNbO_3$, the microwave field was engineered to have a large antisymmetric component, for example by using an electrode on only one side of the WGM resonator[48] or by driving higher order modes of a microwave cavity[40,49]. In x-cut $LiNbO_3$, an alternative approach is possible. Here, the effective nonlinearity for light confined to the rim of the resonator varies azimuthally around the resonator's rim, because the effective $\chi^{(2)}$ is dependent on the direction of the wavevector of the light; the light propagating around the resonator therefore experiences an oscillating $\chi^{(2)}$ (Fig. 1a). This spatial variation allows a uniform microwave field to couple two different spatially orthogonal optical modes from the same mode family. The effective nonlinearities for the modes, $\chi^{(2)}_{\mathrm{eff}}$, are given by the Fourier component of $\chi^{(2)}(\theta)$, which provides the necessary number of momentum quanta (see Supplementary Note 1). For the axial modes we find $\chi^{(2)}_{\mathrm{eff}} = 63.2\,\mathrm{pm\,V^{-1}}$ and for radial modes $\chi^{(2)}_{\mathrm{eff}} = 240\,\mathrm{pm\,V^{-1}}$ for 633 nm light and 50 MHz to 86 MHz modulation frequency. This is comparable to the largest component of the electro-optic tensor $\chi^{(2)}_{33} = 362\,\mathrm{pm\,V^{-1}}$[50], as used in z-cut devices.

Single comb generation. We first characterize the single comb that is generated when a microwave field with a single frequency

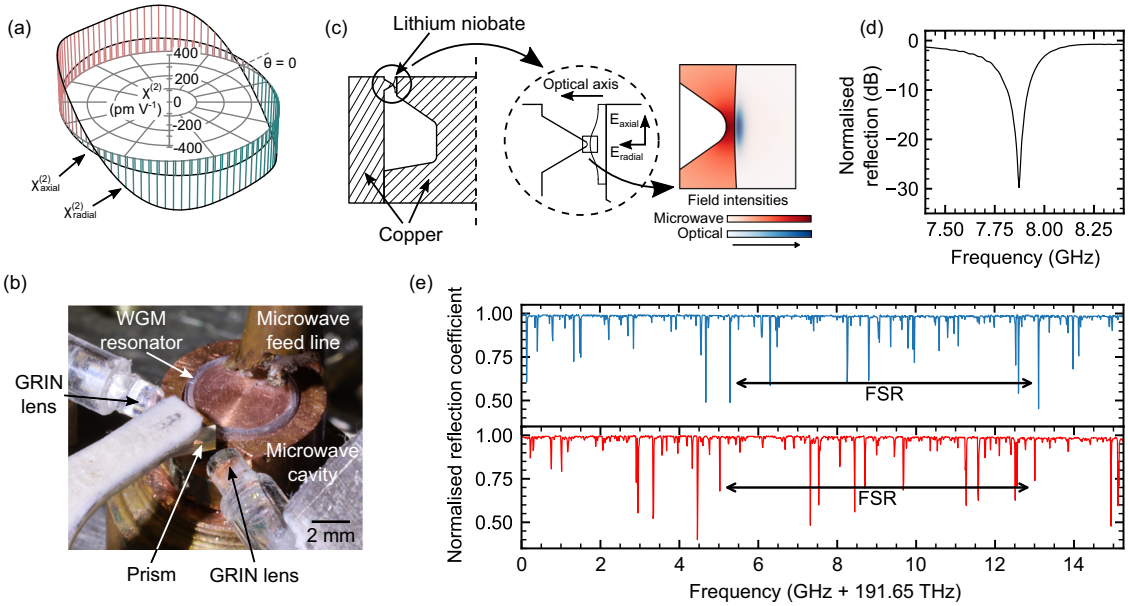

Fig. 1 Device principles and design. a Effective electro-optic coefficient of $LiNbO_3$ for axial and radial modes as a function of angle from the crystallographic *z*-axis, showing the angular dependency. **b** Cartoon of our device, with the $LiNbO_3$ ring embedded in a toroidal loop gap. A gap in the outer of the cavity provides for optical access via prism coupling. **c** Left—half cross-section of the device in **b**. Centre—expanded view of $LiNbO_3$ resonator and the gap of the loop-gap resonator. Right—expanded view of the edge of the resonator and cavity, showing COMSOL simulations of the optical and microwave field intensities. **d** Microwave spectrum of the cavity, tuned to critical coupling. **e** Optical mode spectrum for radial (upper) and axial (lower) modes. Free spectral ranges (FSRs) are arrowed.

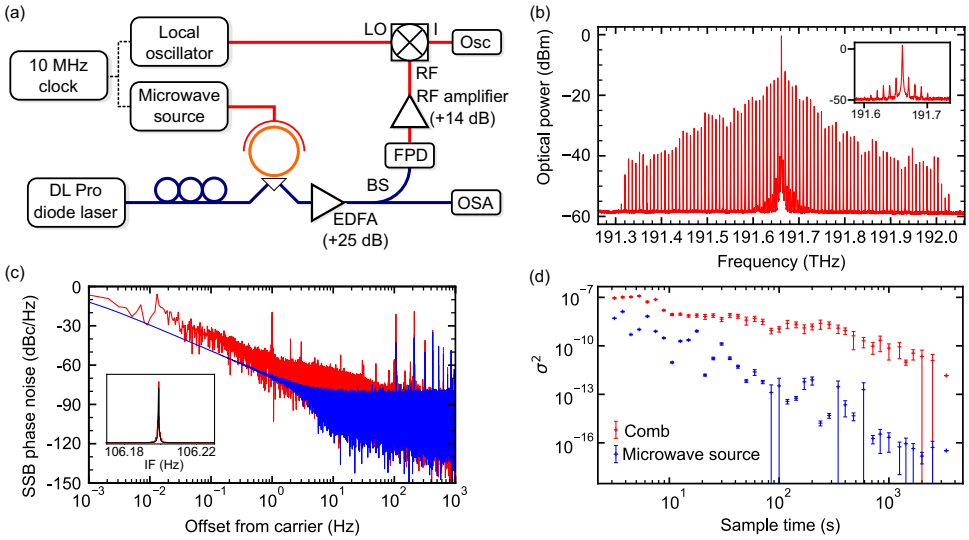

Fig. 2 Single comb generation. a Experimental set-up. The output of a grating-stabilized diode laser is tuned to a mode of a thermally stabilized whispering gallery mode (WGM) resonator, with the input polarization selected using a polarization controller (PC). The surrounding microwave cavity is driven at the free spectral range (FSR) of the optical modes, and the resulting comb is amplified with an erbium-doped fibre amplifier (EDFA) before being split with a beam splitter (BS) and measured with both an optical spectrum analyser (OSA) and a fast photodiode (FPD). The radio-frequency (RF) FPD output is mixed with a local oscillator (LO) detuned by ~100 Hz from the comb repetition rate, and the resulting intermediate frequency (IF) signal digitized using an oscilloscope (Osc). **b** A single frequency comb, with 91 comb lines visible and a repetition rate of 7.940 GHz. **c** Single sideband phase noise of the IF due to a single comb (red) and the microwave drive (blue), as a function of offset from the carrier. Inset is the IF lineshape (red) and a fit to a Lorentzian lineshape (black). **d** Allan variance of the IF due to the comb (red) and the microwave source (blue). Error bars denote one standard deviation.

interacts with the optical field. 1550 nm light from a Toptica DL Pro grating stabilized diode laser is passed through a fibre polarization controller and then coupled into the WGM resonator (major radius = 2.56 mm, minor radius = 400 μm) using a graded index lens and diamond prism (Fig. 2a). The emitted light from the resonator is out-coupled in the same way. We chose here to tune the optical pump to a mode in a radially polarized optical mode family, with Q factors approaching 10^8 and an FSR of 7.940 GHz; we therefore drive the microwave cavity at this frequency, with an incident power on the cavity of 35 dBm. We measure the resulting output spectrum with an optical spectrum analyser and find that a single comb with 91 comb lines is generated (Fig. 2b). From the ratio of the power in adjacent comb lines[40], we estimate the coupling rate to be $g \approx 2\pi \times 0.3$ Hz.

The comb spectrum is cut off abruptly at 191.3 THz and 192.05 THz. At these points dispersion-induced breakdown of the comb occurs, as the intrinsic and geometric dispersion of the resonator results in a change of FSR at large detunings from the centre frequency[40,42]. This results in an offset between the FSR and the frequency of the driving microwave field. At the comb cutoffs, this offset exceeds the electro-optically broadened linewidth of the optical modes, the resonance condition no longer holds, and the cascaded sideband generation process cannot continue.

To measure the stability of the repetition rate of the comb, the intensity of the frequency comb is measured with a fast photodiode (FPD) with a bandwidth of 20 GHz. The output from this carries the beat frequency between comb lines, and the linewidth of this signal is a measure of the comb spacing stability. This linewidth is too small to measure directly using, for example, a microwave spectrum analyser. Instead, we mix this signal with a local oscillator detuned from the microwave source by 106.2 Hz, and study the linewidth of the resulting intermediate frequency (IF) by digitally sampling it and taking the power spectrum of the resulting discrete time signal (see Methods). In Fig. 2c, we show the single sideband (SSB) phase noise of the IF, with its lineshape inset, and in Fig. 2d we show the Allan variance of the IF. For comparison, we also show the phase noise and Allan deviation of the driving microwave source. We find a linewidth of $\sigma_{\mathrm{meas}} = (0.24 \pm 0.07)$ mHz, demonstrating the extremely high stability of the repetition rate of the frequency comb.

Contributions to σ_{meas} come from phase noise on the microwave drive signal and optical phase noise due to the lithium niobate. To quantify these components, we start by directly measuring the linewidth of the microwave drive tone, using the same r.f. measurement chain. We find it to be $\sigma_{\mathrm{mw}} = (0.100 \pm 0.019)$ mHz. The dominant source of the 7.940 GHz microwave signal from the comb is the beat note between the carrier and the two first order comb lines, which are summed coherently. We therefore deduce that noise processes in the lithium niobate contribute an effective linewidth $\sigma_{\mathrm{LN}} = \sqrt{\sigma_{\mathrm{meas}}^2 - \sigma_{\mathrm{mw}}^2} = (0.22 \pm 0.08)$ mHz for the first order comb lines.

Dual comb generation. We now exploit the two polarizations supported in the WGM resonator to generate a dual comb. We begin by using an acousto-optic modulator (AOM) to split the carrier into two equal magnitude carriers separated by 100 MHz (Fig. 3a). These are prepared in orthogonal linear polarization states, and then recombined into a single fibre. The polarizations are then rotated so that they correspond to axial and radial modes in the WGM resonator, and can therefore excite two optical modes of different polarization with centre frequencies 100 MHz apart.

Two microwave tones of powers 32 dBm at 7.814 GHz and 7.934 GHz—commensurate with the FSRs of the axial and radial modes respectively—are then used to excite the mode supported by the metal cavity. Two frequency combs are observed, with comb line spacings equal to the applied microwave tones (Fig. 3b). The longer comb, with more than 50 visible comb lines, forms in the radial mode family, while the axially polarized comb is shorter due to its lower $\chi_{\mathrm{eff}}^{(2)}$.

A key advantage of dual-comb based techniques is that the combs can traverse spatially separated paths, and then be referenced against each other by mixing them down to r.f. frequencies with a fast photodiode. This requires that they can be separated into 'probe' and 'reference' combs; for the output of our device this can be achieved straightforwardly by a polarizing beam splitter (PBS), as the generated combs are orthogonally polarized. In order to mix them together, the reference comb polarization is then rotated by 90° so that it has the same polarization as the probe comb, and they are then recombined with a 3 dB beam splitter before the photodiode.

In Fig. 3c, we show the low frequency regime of the resulting spectrum. We label the peaks with the order of the originating comb lines, with $n = 0$ labelling the beating of the two pump tones. We also observe artefacts at frequencies spaced 100 MHz from IFs due to the combs. These are due to nonlinearities in our detection chain, and the high power present in the 100 MHz zeroth order line resulting from the two optical carriers.

We demonstrate the separability of the two orthogonally polarized combs with a PBS in Fig. 3d. A fibre Bragg grating (FBG) with centre frequency 191.807 THz and bandwidth 40 GHz is introduced into the probe arm. Here we arbitrarily choose to use the 7.934 GHz spaced radially polarized comb as the probe comb. The FBG reflects light from the comb across its bandwidth, resulting in three absent comb lines in the spectrum.

We now examine the relative frequency stability of the two combs constituting the dual comb. The two microwave sources providing the comb spacing frequencies and the 100 MHz r.f. source driving the AOM are locked to the same 10 MHz clock, allowing accurate assessment of the phase noise due to optical noise in the resonator. This is measured in a similar way as for the single comb, by mixing the beat tone between two comb lines with a local oscillator (from a source that is locked to the same 10 MHz clock as the comb sources). This generates an IF of ~100 Hz, which is sampled at a frequency of 10 kHz. The power spectrum of the IF signal is then calculated.

We measure the linewidths for IF orders between 1 and 10. In Fig. 4a, we show the SSB phase noise for the zeroth order IF, resulting from the two optical carriers separated by 100 MHz, and first order IF, generated by comb lines separated by 20 MHz. We also show the SSB phase noise for the microwave drives. In Fig. 4b, we show linewidths as a function of generating comb line pair order. We determine an IF linewidth of (0.217 ± 0.096) mHz for the zeroth order beat note between the two carriers. This originates from uncorrelated noise on the two fibre arms of the output of the AOM. In Fig. 4c, we show the Allan variance of the IF due to the carriers, the first pair of lines, and the driving microwave source.

We find that the IF linewidth rises with increasing comb line pair order. Noise at the repetition rate of one comb is common to all comb lines for that comb. The noise generating processes for each individual comb are therefore correlated between comb lines, but uncorrelated between the two combs and uncorrelated with phase noise due to the AOM. By assuming the magnitude of the microwave frequency noise power at the two FSRs is the same, and there is no other source of dephasing between the two combs we fit

$$\sigma_n^2 = \sigma_{\mathrm{AOM}}^2 + 2n\left(\sigma_{\mathrm{mw}}^2 + \sigma_{\mathrm{LN}}^2\right) \tag{2}$$

to the IF linewidths due to the nth order pair (see Methods). In the limit of large n, this gives $\sigma_n = \sqrt{2n(\sigma_{\mathrm{mw}}^2 + \sigma_{\mathrm{LN}}^2)}$. From our fit we find $\sigma_{\mathrm{LN}} = (0.36 \pm 0.08)$ mHz, consistent within experimental error with the value determined above for the single comb, and supporting the conclusion that there is no significant additional source of dephasing between the combs.

Cross talk between the two constituent combs can be deleterious to dual comb performance because of a reduction in the signal-to-noise ratio[51]. We characterize the cross talk in our device by driving the system with the two microwave tones required for dual comb generation, but pumping an optical mode of only one polarization at a time. The resulting optical

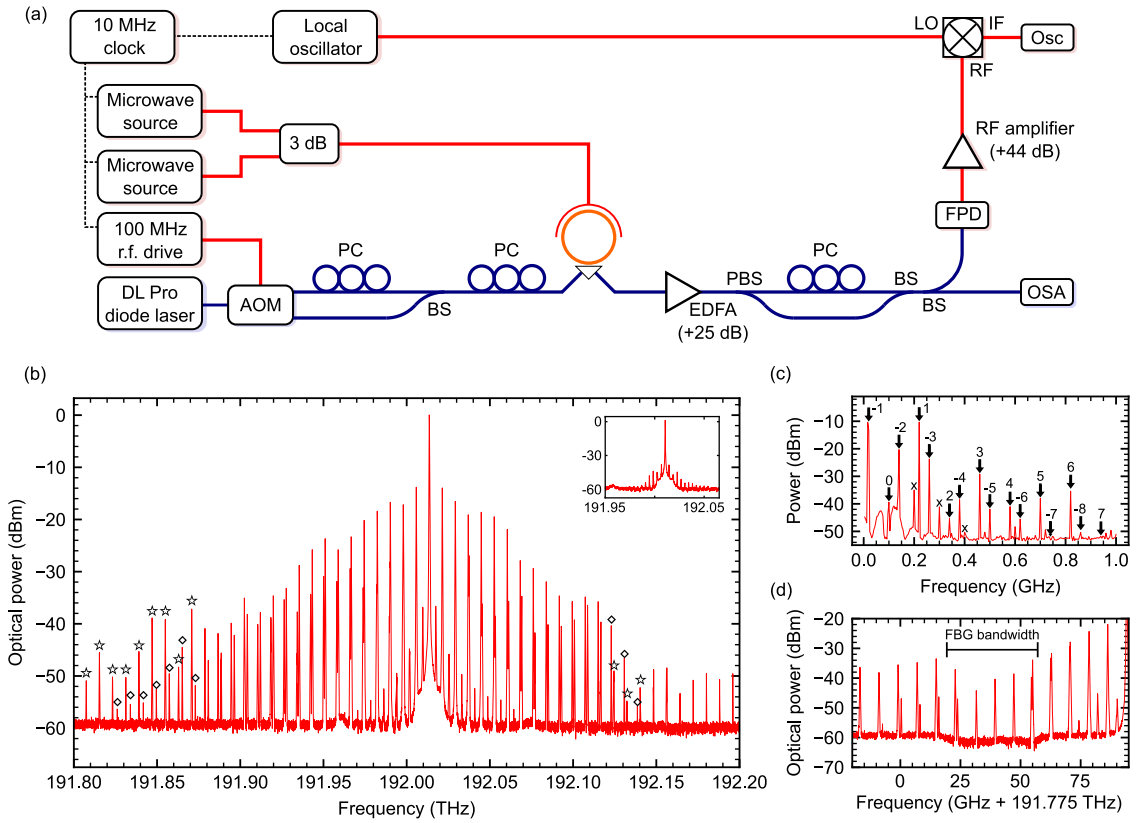

Fig. 3 Dual comb generation. a Experimental set-up for dual comb generation. Two frequencies resonant with modes of orthogonal polarization are generated from a single laser and an acousto-optic modulator (AOM), prepared in the correct polarization states with polarization controllers (PCs), and combined using a beam splitter (BS). The cavity is simultaneously driven at the free spectral range of both mode families. The resulting combs are amplified using an erbium doped fibre amplifier (EDFA) and then separated using a polarizing beam splitter (PBS). The reference comb is then rotated on to the same polarization as the probe before output to the measurement chain comprising an optical spectrum analyser (OSA), fast photodiode (FPD) and oscilloscope (Osc) as for the single comb measurement (Fig. 2). **b** A dual polarization dual comb with line spacings of 7.934 and 7.814 GHz; the individual combs are marked with white star (☆) and white diamond (◇), respectively at large detunings. Also visible is the incomplete suppression of the pump laser sidebands, with spacing 3.94 GHz, forming an incoherent comb—the inset shows the spectrum of the diode laser alone. **c** Mixing of dual comb lines to RF frequencies. Beat frequencies are labelled with the order of the originating comb lines. Artefacts at integer multiples of 100 MHz are marked with a cross. **d** Separability of combs; lines from the 'probe' comb at frequencies between 191.787 and 191.827 GHz are filtered by a fibre Bragg grating (FBG), while the reference comb is not affected.

signal is mixed down to microwave frequencies using an FPD as before. The resulting microwave spectra are shown in Fig. 4d for pumps of axial (upper panel) and radial (lower panel) optical polarization. In both cases, peaks are visible at 7.814 GHz and 7.934 GHz with the cross talk between combs characterized by the contrast between the peaks. We find cross talk less than -30 dB for both axial and radial combs. Cross talk in our system is suppressed by the requirement for new optical frequencies to be resonant with an appropriately polarized mode of the WGM resonator.

The dual comb relative stability we have demonstrated compares favourably to that measured for previous unstabilized dual combs[28,52], and is comparable to dual combs using active stabilization and post-processing techniques[11,17,19,22,23,53–57]. We ascribe the high frequency stability of our generated frequency combs to two principle reasons. Firstly, all our generating frequencies are directly derived from phase stable microwave sources which are all synchronized to the same 10 MHz clock. Secondly, comb generation for both combs takes place in the same optical mode volume, preventing uncorrelated noise generated by thermal or microwave frequency fluctuations in separate microresonators from limiting the coherence between the combs[28,58].

The dual combs shown here have centre frequencies of ~193 THz, and repetition rates of ~8 GHz. The versatility of our technique offers pathways to comb generation in alternative frequency regimes. $LiNbO_3$ is transparent in the range 350 nm to 4.5 μm, but by choosing another electro-optic material with appropriate crystal symmetries different wavelengths could be accessed. For example, mid-IR parts of the spectrum could be accessed by using silver gallium selenide[59], which is transparent to about 18 μm. Alternatively materials such as lithium tetraborate[60] and beta barium borate[61] are transparent to around 250 nm, potentially allowing generation of mid-ultraviolet frequency combs (see Supplementary Note 3).

The desirable repetition rates of dual combs is dependent on the application, and might range from hundreds of MHz for spectroscopy of gases, to many tens of GHz for spectroscopy of solids or liquids, which have broader absorption lines[62]. For resonant electro-optic devices, repetition rates are set by the FSRs of the relevant mode families. These in turn are set by the diameter of the microresonator, and the refractive index and birefringence of the material used. The fabrication of resonators with FSRs of between 0.5 and 25 GHz is readily achievable. We tabulate some examples of material indices, and resulting percentage differences in FSR, in Supplementary Note 3.

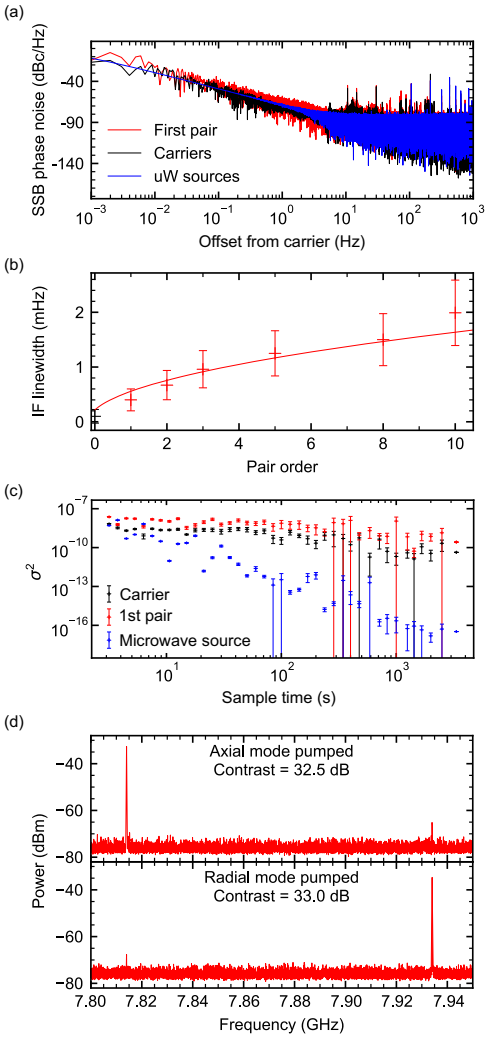

Fig. 4 Characteristics of dual comb. a SSB phase noise of the beat frequencies between the carriers (black) and first order comb lines (red). **b** IF linewidth vs dual comb line pair order. The fitted curve assumes comb broadening due to noise in $\chi^{(2)}$. **c** Allan variance of the IFs due to the carriers (black), the first pair of comb lines (red) and the microwave sources (blue). **d** Cross-talk between single combs. The cavity is driven with microwave tones at both FSRs, while only one optical polarization is pumped. The resulting optical output from the resonator is measured with an FPD and the microwave power at the beat frequency of each comb compared. Error bars denote one standard deviation.

Conclusion

In conclusion, we have demonstrated that the wave-vector dependent nonlinearities present in WGM resonators fabricated from x-cut $LiNbO_3$ can be used to generate frequency combs, which avoids the requirement for a spatially varying microwave field. They also allow the simultaneous generation of two combs, with different comb line spacings and different polarizations. Because of the spatial multiplexing of the two combs, and the fact that phase locked microwave sources control all relevant frequencies, our combs demonstrate high free-running mutual coherence.

Moreover, comb generation is deterministic and start-up speed is limited only by the lifetime of the cavity modes. In addition to slow thermal tuning, rapid fine tuning of the centre frequencies and comb spacings could be achieved by application of a d.c. bias. This device is therefore a step towards a versatile platform for simple and cost effective dual comb generation.

Methods

Sample design and fabrication. The copper microwave cavity was made using standard mechanical techniques in two parts; an inner rod of diameter 5 mm, and an outer cap. To obtain the correct fundamental mode frequency we based the dimensions on design rules for loop gap cavities (see S.I.), with a gap relative permittivity of $\epsilon_r = 57$ representing the x-cut $LiNbO_3$ occupying the electric field mode volume. The initial design was then modelled using COMSOL Multiphysics, and design parameters adjusted accordingly.

A ring-shaped $LiNbO_3$ precursor was cut from a 0.5 mm thick x-cut wafer using grinding techniques; a hollow brass cylinder, of inside diameter 5 mm, was mounted in an air bearing and spun at 100 Hz. It was brought into gentle contact with the $LiNbO_3$, with the cylinder axis normal to the wafer, and diamond slurry (30 μm) added. Once the entire thickness of the wafer had been abraded away, the process was repeated with a larger brass cylinder to form the outer perimeter of the ring.

The precursor was fixed to top of the inner rod of the copper cavity using cyanoacrylate, and carefully levelled. It was then mounted in the air bearing and cut to shape and size using single point diamond turning until around 100 μm thick in the radial direction. Finally, it was mechanically polished by hand, using 1 and 0.25 μm diamond slurry[45–47].

To achieve the required mode frequency, the cavity mode frequency and FSRs of the WGM resonator were measured, the outer cap removed, and a small amount of copper in the loop of the loop-gap removed from the fabricated device.

Linewidth measurement. To measure the relative stability of frequency comb lines, the spectrum generated by the comb was mixed to r.f. intermediate frequencies using a Thorlabs DXM20AF fast photodetector with a 20 GHz bandwidth. To select the intermediate frequency of interest, the r.f. signal was mixed again (Mini-Circuits ZLW-2/ZX05-153LH-S+), with the local oscillator (Rohde and Schwarz SMR20) detuned 106.2 Hz from the expected intermediate frequency. The local oscillator linewidth was determined by mixing against an independent microwave source, and found to be narrower than our measurement floor. The resulting 106.2 Hz signal was low pass filtered (3 dB cutoff of 15 kHz) to avoid aliasing then digitized at a sample rate of 10 kHz. The power spectrum of this signal was then calculated, and the width of the peak at 106.2 Hz determined by fitting a Lorentzian lineshape.

Error analysis for fit. Fitting Eq. (2) to dual comb beat linewidths to determine σ_{LN} requires careful handling of the uncertainties. In particular, σ_{AOM} and σ_{mw} are independently measured parameters in this equation, but also have an uncertainty associated with them. To account for this, we estimate the uncertainty of σ_{LN} by drawing 10000 samples for $\{\sigma_n\}$, σ_{AOM} and σ_{mw} from uncorrelated normal distributions having widths equal to the experimentally measured uncertainties, and then fitting for each set to find estimates for σ_{LN}. The width of the resulting distribution gives the uncertainty on σ_{LN}.

Data availability

The data that are presented in the figures of this paper are available at https://doi.org/10.5281/zenodo.5943157.

Received: 14 September 2022; Accepted: 6 April 2023;
Published online: 03 May 2023

References

1. Diddams, S. A., Vahala, K. & Udem, T. Optical frequency combs: coherently uniting the electromagnetic spectrum. *Science* **369**, eaay3676 (2020).
2. Pfeifle, J. et al. Coherent terabit communications with microresonator Kerr frequency combs. *Nat. Photonics* **8**, 375–380 (2014).
3. Ataie, V. et al. Ultrahigh count coherent WDM channels transmission using optical parametric comb-based frequency synthesizer. *J. Lightwave Technol.* **33**, 694–699 (2015).
4. Papp, S. B. et al. Microresonator frequency comb optical clock. *Optica* **1**, 10–14 (2014).
5. Obrzud, E. et al. A microphotonic astrocomb. *Nat. Photonics* **13**, 31–35 (2019).
6. Lucas, E. et al. Ultralow-noise photonic microwave synthesis using a soliton microcomb-based transfer oscillator. *Nat. Commun.* **11**, 374 (2020).
7. Millot, G. et al. Frequency-agile dual-comb spectroscopy. *Nat. Photonics* **10**, 27–30 (2016).

8. Muraviev, A. V., Smolski, V. O., Loparo, Z. E. & Vodopyanov, K. L. Massively parallel sensing of trace molecules and their isotopologues with broadband subharmonic mid-infrared frequency combs. *Nat. Photonics* **12**, 209–214 (2018).
9. Shams-Ansari, A. et al. Thin-film lithium-niobate electro-optic platform for spectrally tailored dual-comb spectroscopy. *Commun. Phys.* **5**, 1–8 (2022).
10. Vicentini, E., Wang, Z., van Gasse, K., Hänsch, T. W. & Picqué, N. Dual-comb digital holography with high spectral resolution. In: *Conference on Lasers and Electro-Optics (2021), Paper SM1G.1* (Optical Society of America, 2021).
11. Coddington, I., Swann, W. C. & Newbury, N. R. Coherent dual-comb spectroscopy at high signal-to-noise ratio. *Phys. Rev. A* **82**, 043817 (2010).
12. Suh, M.-G., Yang, Q.-F., Yang, K. Y., Yi, X. & Vahala, K. J. Microresonator soliton dual-comb spectroscopy. *Science* **354**, 600–603 (2016).
13. Ycas, G. et al. High-coherence mid-infrared dual-comb spectroscopy spanning 2.6 to 5.2 μm. *Nat. Photonics* **12**, 202–208 (2018).
14. Nürnberg, J., Willenberg, B., Phillips, C. R. & Keller, U. Dual-comb ranging with frequency combs from single cavity free-running laser oscillators. *Opt. Express* **29**, 24910–24918 (2021).
15. Kang, J., Feng, P., Li, B. & Wong, K. K. Y. Dual-comb optical coherence tomography. In: *Advanced Photonics 2018 (BGPP, IPR, NP, NOMA, Sensors, Networks, SPPCom, SOF) (2018), Paper SeTu3H.2* (Optical Society of America, 2018).
16. Nishiyama, A. et al. Doppler-free dual-comb spectroscopy of Rb using optical-optical double resonance technique. *Opt. Express* **24**, 25894–25904 (2016).
17. Coddington, I., Swann, W. C., Nenadovic, L. & Newbury, N. R. Rapid and precise absolute distance measurements at long range. *Nat. Photonics* **3**, 351–356 (2009).
18. Suh, M.-G. & Vahala, K. J. Soliton microcomb range measurement. *Science* **359**, 884–887 (2018).
19. Trocha, P. et al. Ultrafast optical ranging using microresonator soliton frequency combs. *Science* **359**, 887–891 (2018).
20. Parriaux, A., Hammani, K. & Millot, G. Electro-optic frequency combs. *Adv. Opt. Photonics* **12**, 223–287 (2020).
21. Coddington, I., Swann, W. C. & Newbury, N. R. Coherent multiheterodyne spectroscopy using stabilized optical frequency combs. *Phys. Rev. Lett.* **100**, 013902 (2008).
22. Ideguchi, T., Poisson, A., Guelachvili, G., Picqué, N. & Hänsch, T. W. Adaptive real-time dual-comb spectroscopy. *Nat. Commun.* **5**, 3375 (2014).
23. Roy, J., Deschênes, J.-D., Potvin, S. & Genest, J. Continuous real-time correction and averaging for frequency comb interferometry. *Opt. Express* **20**, 21932–21939 (2012).
24. Del'Haye, P. et al. Optical frequency comb generation from a monolithic microresonator. *Nature* **450**, 1214–1217 (2007).
25. He, Y. et al. Self-starting bi-chromatic $LiNbO_3$ soliton microcomb. *Optica* **6**, 1138–1144 (2019).
26. Fang, Z. et al. Efficient electro-optical tuning of an optical frequency microcomb on a monolithically integrated high-Q lithium niobate microdisk. *Opt. Lett.* **44**, 5953–5956 (2019).
27. Yang, Q.-F., Yi, X., Yang, K. Y. & Vahala, K. Counter-propagating solitons in microresonators. *Nat. Photonics* **11**, 560–564 (2017).
28. Lucas, E. et al. Spatial multiplexing of soliton microcombs. *Nat. Photonics* **12**, 699–705 (2018).
29. Kippenberg, T. J., Gaeta, A. L., Lipson, M. & Gorodetsky, M. L. Dissipative Kerr solitons in optical microresonators. *Science* **361**, eaan8083 (2018).
30. Kovacich, R. P., Sterr, U. & Telle, H. R. Short-pulse properties of optical frequency comb generators. *Appl. Opt.* **39**, 4372–4376 (2000).
31. Amiune, N. et al. Optical-parametric-oscillation-based $\chi^{(2)}$ frequency comb in a lithium niobate microresonator. *Opt. Express* **29**, 41378–41387 (2021).
32. Szabados, J. et al. Frequency comb generation via cascaded second-order nonlinearities in microresonators. *Phys. Rev. Lett.* **124**, 203902 (2020).
33. Villois, A., Kondratiev, N., Breunig, I., Puzyrev, D. N. & Skryabin, D. V. Frequency combs in a microring optical parametric oscillator. *Opt. Lett.* **44**, 4443–4446 (2019).
34. Hendry, I. et al. Experimental observation of internally pumped parametric oscillation and quadratic comb generation in a $\chi^{(2)}$ whispering-gallery-mode microresonator. *Opt. Lett.* **45**, 1204–1207 (2020).
35. Mosca, S. et al. Modulation instability induced frequency comb generation in a continuously pumped optical parametric oscillator. *Phys. Rev. Lett.* **121**, 093903 (2018).
36. Hansson, T. et al. Singly resonant second-harmonic-generation frequency combs. *Phys. Rev. A* **95**, 013805 (2017).
37. Leo, F. et al. Frequency-comb formation in doubly resonant second-harmonic generation. *Phys. Rev. A* **93**, 043831 (2016).
38. Kourogi, M., Nakagawa, K. & Ohtsu, M. Wide-span optical frequency comb generator for accurate optical frequency difference measurement. *IEEE J. Quant. Electron.* **29**, 2693–2701 (1993).
39. Beha, K. et al. Electronic synthesis of light. *Optica* **4**, 406–411 (2017).
40. Rueda, A., Sedlmeir, F., Kumari, M., Leuchs, G. & Schwefel, H. G. L. Resonant electro-optic frequency comb. *Nature* **568**, 378–381 (2019).
41. Durán, V., Andrekson, P. A. & Torres-Company, V. Electro-optic dual-comb interferometry over 40 nm bandwidth. *Opt. Lett.* **41**, 4190–4193 (2016).
42. Zhang, M. et al. Broadband electro-optic frequency comb generation in a lithium niobate microring resonator. *Nature* **568**, 373–377 (2019).
43. Grudinin, I. S. et al. Ultra high Q crystalline microcavities. *Opt. Commun.* **265**, 33–38 (2006).
44. Strekalov, D. V., Marquardt, C., Matsko, A. B., Schwefel, H. G. L. & Leuchs, G. Nonlinear and quantum optics with whispering gallery resonators. *J. Opt.* **18**, 123002 (2016).
45. Trainor, L. S., Sedlmeir, F., Peuntinger, C. & Schwefel, H. G. L. Selective coupling enhances harmonic generation of whispering-gallery modes. *Phys. Rev. Appl.* **9**, 024007 (2018).
46. Sedlmeir, F., Hauer, M., Fürst, J. U., Leuchs, G. & Schwefel, H. G. L. Experimental characterization of an uniaxial angle cut whispering gallery mode resonator. *Opt. Express* **21**, 23942–23949 (2013).
47. Fürst, J., Sturman, B., Buse, K. & Breunig, I. Whispering gallery resonators with broken axial symmetry: theory and experiment. *Opt. Express* **24**, 20143–20155 (2016).
48. Ilchenko, V. S., Savchenkov, A. A., Matsko, A. B. & Maleki, L. Whispering-gallery-mode electro-optic modulator and photonic microwave receiver. *J. Opt. Soc. Am. B* **20**, 333–342 (2003).
49. Rueda, A. et al. Efficient microwave to optical photon conversion: an electro-optical realization. *Optica* **3**, 597–604 (2016).
50. Turner, E. H. High-frequency electro-optic coefficients of lithium niobate. *Appl. Phys. Lett.* **8**, 303–304 (1966).
51. Coddington, I., Newbury, N. & Swann, W. Dual-comb spectroscopy. *Optica* **3**, 414–426 (2016).
52. Huh, J. H., Chen, Z., Vicentini, E., Hänsch, T. W. & Picqué, N. Time-resolved dual-comb spectroscopy with a single electro-optic modulator. *Opt. Lett.* **46**, 3957–3960 (2021).
53. Gu, C. et al. Passive coherent dual-comb spectroscopy based on optical-optical modulation with free running lasers. *PhotoniX* **1**, 7 (2020).
54. Kwon, D., Jeon, I., Lee, W.-K., Heo, M.-S. & Kim, J. Generation of multiple ultrastable optical frequency combs from an all-fiber photonic platform. *Sci. Adv.* **6**, eaax4457 (2020).
55. Ideguchi, T., Nakamura, T., Kobayashi, Y. & Goda, K. Kerr-lens mode-locked bidirectional dual-comb ring laser for broadband dual-comb spectroscopy. *Optica* **3**, 748–753 (2016).
56. Chen, Z., Yan, M., Hänsch, T. W. & Picqué, N. A phase-stable dual-comb interferometer. *Nat. Commun.* **9**, 3035 (2018).
57. Zhu, Z., Ni, K., Zhou, Q. & Wu, G. Two-color phase-stable dual-comb ranging without precise environmental sensing. *Opt. Express* **27**, 4660–4671 (2019).
58. Soriano-Amat, M. et al. Common-path dual-comb spectroscopy using a single electro-optic modulator. *J. Lightwave Technol.* **38**, 5107–5115 (2020).
59. Meisenheimer, S.-K., Fürst, J. U., Buse, K. & Breunig, I. Continuous-wave optical parametric oscillation tunable up to an 8 μm wavelength. *Optica* **4**, 189–192 (2017).
60. Fürst, J. U. et al. Second-harmonic generation of light at 245 nm in a lithium tetraborate whispering gallery resonator. *Opt. Letter.s* **40**, 1932–1935 (2015).
61. Lin, G., Fürst, J., Strekalov, D. V., Grudinin, I. S. & Yu, N. High-Q UV whispering gallery mode resonators made of angle-cut BBO crystals. *Opt. Express* **20**, 21372–21378 (2012).
62. Picqué, N. & Hänsch, T. W. Frequency comb spectroscopy. *Nat. Photonics* **13**, 146–157 (2019).

Acknowledgements

N.J.L. is supported by the MBIE (New Zealand) Endeavour Fund (UOOX1805). We also acknowledge support from the Marsden Fund Grant no. 20-UOO-080. We gratefully acknowledge comments on the manuscript from Dr. James Haigh, A. Professor Miro Erkintalo, A. Professor Jevon Longdell, A. Professor Stuart Murdoch, and Dr. Nathalie Picqué.

Author contributions

All authors conceptualized the experiment. N.J.L. fabricated the devices and performed the measurements. N.J.L. and L.S.T. carried out analysis. All authors contributed to writing the manuscript. The project was supervised by H.G.L.S.

Competing interests

The authors have filed a provisional patent application for aspects of this work at the United States Patent and Trademark Office (application number 63216484). The authors declare no other competing interests.

Additional information

Supplementary information The online version contains supplementary material available at https://doi.org/10.1038/s42005-023-01197-x.

Correspondence and requests for materials should be addressed to Nicholas J. Lambert or Harald G. L. Schwefel.

Peer review information *Communications Physics* thanks Tao Lu and the other, anonymous, reviewer(s) for their contribution to the peer review of this work.

Reprints and permission information is available at http://www.nature.com/reprints

Publisher's note Springer Nature remains neutral with regard to jurisdictional claims in published maps and institutional affiliations.

Open Access This article is licensed under a Creative Commons Attribution 4.0 International License, which permits use, sharing, adaptation, distribution and reproduction in any medium or format, as long as you give appropriate credit to the original author(s) and the source, provide a link to the Creative Commons license, and indicate if changes were made. The images or other third party material in this article are included in the article's Creative Commons license, unless indicated otherwise in a credit line to the material. If material is not included in the article's Creative Commons license and your intended use is not permitted by statutory regulation or exceeds the permitted use, you will need to obtain permission directly from the copyright holder. To view a copy of this license, visit http://creativecommons.org/licenses/by/4.0/.

© The Author(s) 2023